Construction and Building Materials 365 (2023) 130087

Contents lists available at ScienceDirect

Construction and Building Materials

journal homepage: www.elsevier.com/locate/conbuildmat

Recycled granulates manufacturing from spent refractory wastes and magnesium based binder

A. Seco [a,d,*], J.M. del Castillo [a,d], C. Perlot [b,c], S. Marcelino [a,d], S. Espuelas [a,d]

[a] Institute of Smart Cities, Public University of Navarre, 31006 Pamplona, Spain
[b] Université de Pau et des Pays de l'Adour, E2S UPPA, SIAME, 64600 Anglet, France
[c] Institut Universitaire de France, France
[d] Dept. of Engineering, Public University of Navarre, 31006 Pamplona, Spain

ARTICLE INFO

Keywords:
Spent refractory wastes
Magnesium oxide
GGBS
Granulation
Carbonation

ABSTRACT

This paper analyzes the ability of two Spent Refractory Wastes (SRW) for the manufacturing of recycled granulates for construction applications. A binary magnesium oxide and ground granulated blast furnace slag hydraulic binder was considered as an agglomerating agent for the granulates manufacturing. Influence of curing atmosphere was carried out: in air, 20 % CO_2 and 100 % CO_2 atmosphere up to 28 days. Granulometry, thermal analysis, particle density, bulk density, water absorption and mechanical strength tests were performed to characterize the granulates. SRW showed their ability for the granulates manufacturing. Results demonstrated the existence of a residual reactivity of the wastes considered. A direct relationship between the CO_2 content of the curing atmosphere and the granulates hydration degree was observed. Carbonation process increased from 7 days to 28 days and direct relationships were observed between the CO_2 content and the carbonation degree as well as between the binder dosage and the carbonation degree. CO_2 curing reduced the water absorption and increased the compressive strength of the granulates.

1. Introduction

Magnesia refractories are indispensable lining materials of high temperature vessels for steel manufacturing. They are ceramic materials mainly composed of periclase, obtained from calcined magnesite, that coat the inside of vessels to withstand the high temperatures reached by the molted metal during the production process. This industry consumes between 8 kg and 15 kg of refractory materials per ton of manufactured steel [1,2]. The EU is the second largest producer of steel in the world after China with an output of over 177 million tons per year [3]. This represents an estimated production of spent refractories between 1.42 and 2.66 million tons a year, in the EU alone. For the last two decades, the interest in the valorization of spent refractories has increased due to environmental regulations, increasing costs for landfilling and raw materials preservation. Magnesia spent refractories are composed of two main fractions, with different characteristics, depending on their exposure to the molten metal. The outer refractory part, that has been in contact with the molten metal, shows slag and metal penetration through the periclase recrystallization cracks. This fraction contains a loss of magnesia and higher silicon concentration because of its migration from the refractory inside to the outside magnesia refractory part. On the other hand, the inner part, which has not been in contact with the molten metal, shows a chemical composition that does not differ much from the refractory nominal composition. The sintering differences generated by the lower temperatures it is submitted to makes the inner part more friable than the outer one [1]. Previous to their valorization, refractory debris require a selection and cleaning process. It is usually carried out by means of a crushing, screening, magnetic separation and eventually a color separation, with the aim of removing impurities such as iron, slag and unwanted pieces of refractory material [2].

The selection and cleaning of these wastes allows the recuperation of metal and the recycling of the majority of the inner part of the spent refractories. This process generates a secondary refractory waste (SRW) composed of the mix of the outer fraction of spent refractory, contaminated with slag and steel as well as with dust particles generated during inner and outer fractions crushing and handling. Nowadays, the recycled fraction is used for the production of new refractories while the secondary wastes lack any effective valorization ways. A possibility for its

* Corresponding author.
E-mail addresses: andres.seco@unavarra.es (A. Seco), jesusmaria.delcastillo@unavarra.es (J.M. del Castillo), celine.perlot@univ-pau.fr (C. Perlot), sara.marcelino@unavarra.es (S. Marcelino), sandra.espuelas@unavarra.es (S. Espuelas).

https://doi.org/10.1016/j.conbuildmat.2022.130087
Received 9 September 2022; Received in revised form 3 November 2022; Accepted 13 December 2022
Available online 23 December 2022
0950-0618/© 2023 The Authors. Published by Elsevier Ltd. This is an open access article under the CC BY license (http://creativecommons.org/licenses/by/4.0/).

Table 1
Chemical composition, reactivity and mineralogy of the spent refractory materials and binder constituents.

Chemical composition (X-ray Fluorescence)				
%	*P*1	*P*2	PC-8	GGBS
SiO_2	2.07	16.53	2.80	32.18
CaO	3.49	12.51	9.10	43.94
Fe_2O_3	1.16	10.99	2.34	0.33
Al_2O_3	2.81	13.69	0.57	10.40
SO_3	0.16	0.31	6.27	2.00
Cr_2O_3	0.04	0.43	–	–
P_2O_5	0.14	0.09	–	–
MnO	0.00	1.95	–	–
MgO	76.13	41.11	59.67	0.25
Reactivity				
L.I. 1050 °C (%)	14.00	1.86	19.25	0.46
Free lime (%)	0.84	–	1.32	0.28
Reactivity (min)	>1200	>1200	>1416	>480
pH	11.37	11.69	10.66	9.82

valorization would be the production of artificial aggregates for the construction industry [4]. However, these secondary wastes have limited recyclability as aggregates for construction purposes because of: (i) their small particle size (according to the processusually under 3 mm) and poor mechanical properties which make them unsuitable for replacing fine aggregates, (ii) their free lime (CaO), reactive magnesium oxide (MgO) and calcium silicate (CS) contents, which are associated with deleterious hydration and carbonation processes with expansive effects and volume instability, and (iii) their high pH. These shortcomings for the direct use of the SRW as aggregates could be overcome by means of the waste granulation with a binder, with or without an accelerated carbonation process [5–12]. This way, recycled aggregates with adequate size would be produced, where a binder and CS would hydrate, contributing to the improvement of the aggregates mechanical properties and CaO and MgO could carbonate, creating a denser structure and contributing to the development of mechanical properties.

This article analyzes the ability of SRW for the production of artificial aggregates. A binary hydraulic binder composed of a low-grade magnesium oxide (MgO) and Ground Granulated Blast-furnace Slag (GGBS) was considered. Different binder dosages and CO_2 curing conditions were investigated. A laboratory investigation was carried out to evaluate the aggregates density, granulate size distribution, strength, water absorption and durability with and without accelerated carbonation. Thermo Gravimetric Analysis (TG/DTG) tests were conducted to elucidate the carbonation degree of the treated samples.

2. Materials and methods

2.1. Materials

Two kinds of SRW were considered in this work, named respectively P1 and P2. P1 is generated during the recovery process of refractory bricks from a ladle furnace, while P2 comes from the demolition of a foundry molten steel distribution vessel named “tundish”. Table 1 shows the chemical composition and reactivity parameters of both materials as well as of the magnesium-based binary binder’s constituents (PC-8 + GGBS). Fig. 1 depicts the granulometric curves of all the materials considered in this investigation.

Based on X-ray Diffraction tests *P*1 mineralogy was estimated mainly as periclase and, to a lower extent, portlandite and CS. *P*2 contains periclase, monticellite, merwinite, forsterite, magnesioferrite and magnesium iron aluminum oxide. Both refractory wastes could maintain some reactivity that would provoke their instability. This, in addition to their small particle size, makes it necessary for treatment before their use, to be suitable as recycled aggregates for construction.

The binary hydraulic binder was composed of a co-product of low grade MgO, marketed by *Magnesitas Navarras S.A*. Co. under the name PC-8, and GGBS as a source of reactive Si and Al at a ratio of 20 to 80, based on previous experiments [13,14]. PC-8 is a magnesium dust recovered from kilns, where calcined magnesite is produced. This dust contains a mix of unburned magnesite, calcined MgO and eventually sintered MgO, depending on the part of the combustion chamber where they were pulled from and the higher temperature they were exposed to. GGBS is a by-product obtained during the manufacturing of pig iron. It is formed by rapid cooling of molten iron slag to maintain an amorphous structure and ground in order to increase its specific surface area (SSA). The sample available for this investigation was provided by Heidelberg Cement Group (UK). As shown in Table 1, GGBS has a huge cementitious potential due to its richness in reactive calcium, silicon, and aluminum oxides.

2.2. Samples manufacturing

Dry SRW and binder constituents were pre-mixed in a laboratory mixer for 5 min to guarantee a complete homogenization. The waste to binder ratios considered were 90 to 10, 80 to 20 and 70 to 30 [11,15–17]. Once the mix was homogenized, 2 kg were poured in the granulator. It was 600 mm in diameter, 370 mm in collar height and was equipped with a blade. Granulation was performed under laboratory conditions. The revolution speed for granulating was set at 50 rpm with a tilting angle of 15°. Once the granulator had been turned on, 400 g of deionized water were sprayed in the granulator (water to solid ratio of

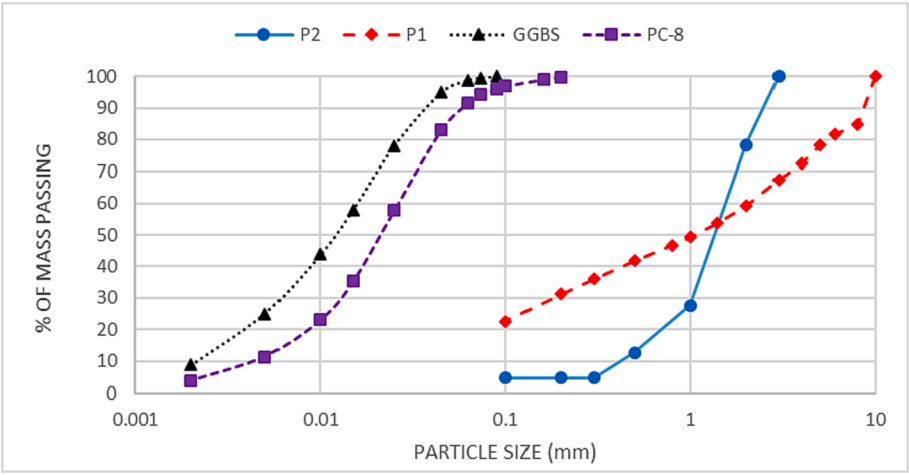

Fig. 1. Granulometric curves of the spent refractory materials and the binder constituents.

Table 2
Granulate combinations manufactured.

COMBINATION	SRW KIND	SRW MASS (g)	BINDER MASS (g)	WATER MASS (g)	CURING TIME (days)	CURING ATMOSPHERE
*P*1/10/7/A	*P*1	900	100	200	7	Air
*P*1/20/7/A	*P*1	800	200	200	7	
*P*1/30/7/A	*P*1	700	300	200	7	
*P*1/10/28/A	*P*1	900	100	200	28	
*P*1/20/28/A	*P*1	800	200	200	28	
*P*1/30/28/A	*P*1	700	300	200	28	
*P*1/10/7/C20	*P*1	900	100	200	7	CO_2 20 % N_2 80 %
*P*1/20/7/ C20	*P*1	800	200	200	7	
*P*1/30/7/ C20	*P*1	700	300	200	7	
*P*1/10/28/ C20	*P*1	900	100	200	28	
*P*1/20/28/ C20	*P*1	800	200	200	28	
*P*1/30/28/ C20	*P*1	700	300	200	28	
*P*1/10/7/C100	*P*1	900	100	200	7	CO_2 100 %
*P*1/20/7/ C100	*P*1	800	200	200	7	
*P*1/30/7/ C100	*P*1	700	300	200	7	
*P*1/10/28/ C100	*P*1	900	100	200	28	
*P*1/20/28/ C100	*P*1	800	200	200	28	
*P*1/30/28/ C100	*P*1	700	300	200	28	
*P*2/10/7/A	*P*2	900	100	200	7	Air
*P*2/20/7/A	*P*2	800	200	200	7	
*P*2/30/7/A	*P*2	700	300	200	7	
*P*2/10/28/A	*P*2	900	100	200	28	
*P*2/20/28/A	*P*2	800	200	200	28	
*P*2/30/28/A	*P*2	700	300	200	28	
*P*2/10/7/C20	*P*2	900	100	200	7	CO_2 20 % N_2 80 %
*P*2/20/7/ C20	*P*2	800	200	200	7	
*P*2/30/7/ C20	*P*2	700	300	200	7	
*P*2/10/28/ C20	*P*2	900	100	200	28	
*P*2/20/28/ C20	*P*2	800	200	200	28	
*P*2/30/28/ C20	*P*2	700	300	200	28	
*P*2/10/7/C100	*P*2	900	100	200	7	CO_2 100 %
*P*2/20/7/ C100	*P*2	800	200	200	7	
*P*2/30/7/ C100	*P*2	700	300	200	7	
*P*2/10/28/ C100	*P*2	900	100	200	28	
*P*2/20/28/ C100	*P*2	800	200	200	28	
*P*2/30/28/ C100	*P*2	700	300	200	28	

0.2) during one minute, and granulation continued for 10 min to complete the granulates formation process [18]. This procedure was repeated three times for each combination, to obtain the necessary amount of granulates. Afterwards, granulates were collected and cured in natural air atmosphere, as well as in atmospheres composed of 20 % CO_2 and 80 % N_2, and in 100 % CO_2, until the testing ages of 7 and 28 days. Before testing, samples were dried at 105 °C for 24 h. A total of 36 combinations were manufactured. Each combination was designated by the code SRW/BP/CT/CA being:

SRW waste type (*P*1, *P*2).
BP binder percentage (10 %, 20 %, 30 %).
CT curing time (7 days, 28 days).

Fig. 2. Appearance of manufactured granulates.

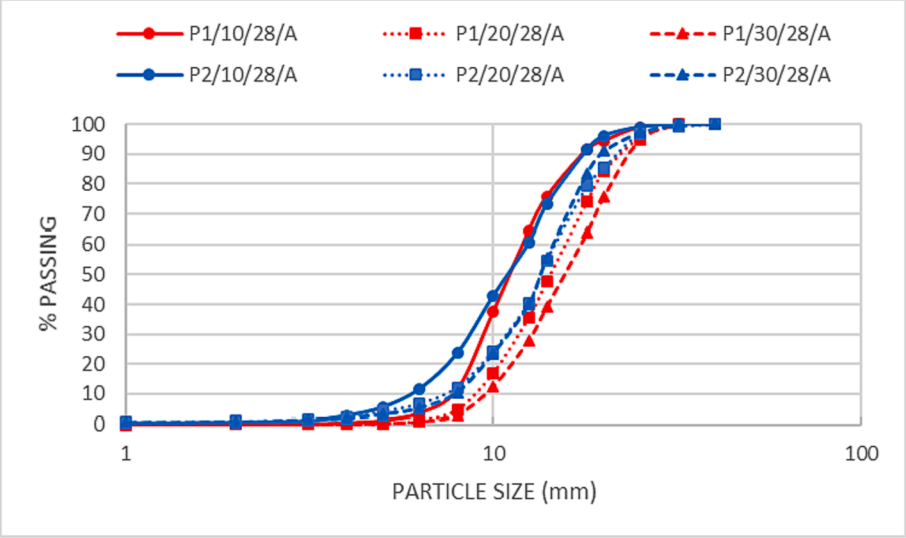

Fig. 3. Granulometric curves of the granulates manufactured.

CA curing atmosphere (air, CO_2 20 %, CO_2 100 %).

Table 2 shows the combinations produced, their composition and the curing atmosphere.

2.3. Samples testing

Granulate particles size distribution was obtained through sieving test with square-opening sieves in accordance with the standard EN 933–1. TG/DTG tests were used to analyze the chemical composition within decomposition of samples against temperature. This test was carried out with 30 mg of sample from 25 °C to 900 °C in nitrogen atmosphere with a flux rate of 100 ml/minute. Bulk density was determined in accordance with the standard UNE-EN 1097–3, eliminating particles bigger than 20 mm. Particle density and water absorption were determined in accordance with the standard UNE-EN 1097–6, through the hydrostatic weighing method. Particle sizes smaller than 4 mm and>20 mm were not considered in this test. Granulate strength was measured using the single pellet crushing method [11]. 40 granulates of 14–18 mm diameter of each combination were used for this test. The fracture load of each single granulate was calculated according to the standard ISO 8942. The samples mechanical strengths were obtained as the mean value of dividing the fracture loads by the granulate areas at the maximum diameter section.

3. Results and discussion

3.1. Granulates particle size distribution

Fig. 2 shows the granulates appearance after manufacturing. Fig. 3 depicts the aggregates granulometric particles size distribution of the air cured combinations at the age of 28 days.

As expected, granulates were mostly spherical, demonstrating that the considered granulation time was enough to complete the layering over the agglomeration process [12]. All the combinations showed continuously graded granulometric curves with>95 % of the granulate sizes in the range 3.15/25 mm, in accordance with other authors like Azrar et al. [19]. The relation between the granulate maximum and minimum diameters is in all the combinations>1.4 ($D/d \geq 1.4$), accomplishing the requirements of the Spanish standard for structural concrete EHE08. For both SRW wastes, granulates diameter increased as the binder content did: *P*2/10/28/A reached the finest granulate sizes and *P*1/30/28/A the coarsest ones, demonstrating the effect of the binder dosage in the granulates size distribution and the ability of *P*1 to produce aggregates with greater diameter than *P*2.

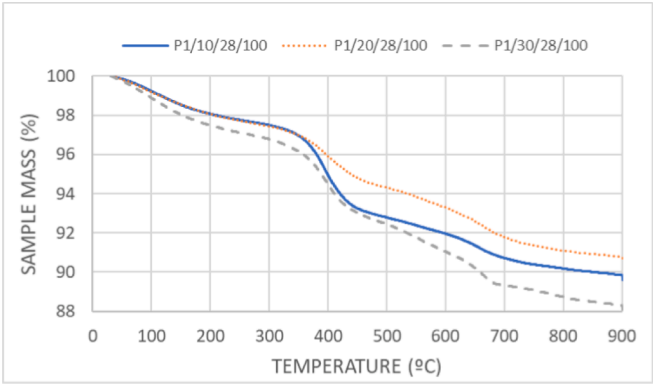

a)

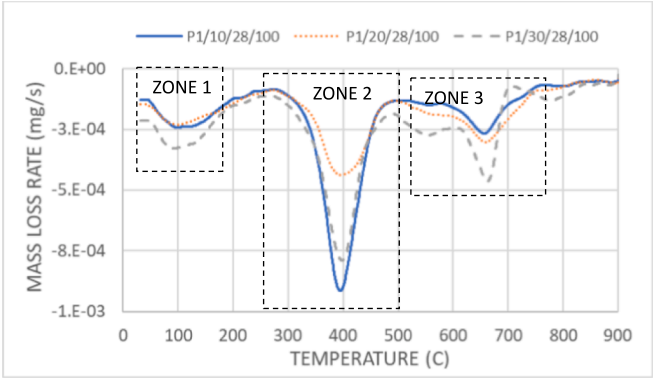

b)

Fig. 4. Decomposition curves against temperature of *P*1 samples at 28 days, with 10 %, 20 % and 30 % of binder dosage, cured in 100 % CO_2 atmosphere. a) TG curves, b) DTG curves.

3.2. Chemical composition

TG/DTG tests were carried out to analyze chemical composition of the granulates within their decomposition of samples against

Table 3
Percentages of mass losses for each combination related to the dehydration, dehydroxylation and decarbonation processes.

COMBINATION	ZONE 1 DEHYDRATION (50 °C-200 °C)	ZONE 2DEHYDROXILATION (250 °C-500 °C)	ZONE 3 DECARBONATION (500 °C-750 °C)
	% of total mass	% of total mass	% of total mass
*P*1/10/7/A	0.00	2.29	2.14
*P*1/20/7/A	1.27	2.34	2.82
*P*1/30/7/A	1.64	3.42	3.42
*P*1/10/28/A	1.00	2.27	2.09
*P*1/20/28/A	1.23	2.25	2.76
*P*1/30/28/A	1.41	2.34	3.37
*P*1/10/7/C20	1.15	2.66	2.31
*P*1/20/7/C20	1.75	3.82	2.57
*P*1/30/7/C20	1.72	2.60	2.93
*P*1/10/28/C20	1.41	3.18	2.58
*P*1/20/28/C20	1.81	3.32	3.12
*P*1/30/28/C20	1.83	3.05	3.26
*P*1/10/7/C100	2.14	5.32	2.41
*P*1/20/7/C100	2.03	4.77	2.77
*P*1/30/7/C100	2.39	4.96	3.07
*P*1/10/28/C100	1.79	4.97	2.39
*P*1/20/28/C100	1.78	3.40	2.96
*P*1/30/28/C100	2.26	4.67	3.36
*P*2/10/7/A	0.51	0.56	1.35
*P*2/20/7/A	0.85	1.03	1.99
*P*2/30/7/A	0.83	1.10	2.31
*P*2/10/28/A	0.58	0.59	1.44
*P*2/20/28/A	0.77	1.01	1.97
*P*2/30/28/A	1.04	1.28	2.39
*P*2/10/7/C20	0.65	0.73	1.44
*P*2/20/7/ C20	1.12	1.30	2.06
*P*2/30/7/C20	1.20	1.45	2.70
*P*2/10/28/C20	1.00	1.15	1.78
*P*2/20/28/C20	1.28	1.47	2.05
*P*2/30/28/C20	1.46	1.66	3.04
*P*2/10/7/C100	1.94	3.96	2.44
*P*2/20/7/C100	1.40	2.25	2.24
*P*2/30/7/C100	1.72	2.75	2.59
*P*2/10/28/C100	1.45	2.32	2.75
*P*2/20/28/C100	2.22	4.20	3.14
*P*2/30/28/C100	2.08	3.36	3.52

temperature. TG curves showed the mass loss at the different temperature ranges (Fig. 4a). DTG curves (Fig. 4b) were used to identify the ranges of temperatures at which dehydration, dehydroxylation and decarbonation processes occur [20]. Fig. 4 shows as an example the TG/DTG curves of *P*1 samples at 28 days, with 10 %, 20 % and 30 % of binder dosage, cured in 100 % CO_2 atmosphere.

The three decomposition characteristic zones of the cementitious products were observed in DTG curves [21,22]. In this investigation zone 1 ranged between 50 °C and 200 °C, corresponding to the loss of free water and water physically adsorbed in hydration products like CSH and MSH gels [12,21,22], which therefore corresponds to the dehydration zone. Zone 2 comprised the temperature range between 250 °C and 500 °C. This region corresponded to the dehydroxylation of Ca$(OH)_2$ and Mg$(OH)_2$ [8,12,23,24]. The third decomposition zone was identified in the range between 500 °C and 750 °C [12,20,25,26] as decarbonation zone. The main peak of this zone, due to the decomposition of calcium carbonates $CaCO_3$, was centered at about 650 °C. Fig. 4b shows how a secondary peak centered at about 550 °C appeared in zone 3, more clearly for the dosage of 30 %. This result was attributed to the decomposition of magnesium carbonate $MgCO_3$.

Table 3 shows the percentages of mass losses for each combination obtained in the TG curves related to the dehydration, dehydroxylation and decarbonation processes previously defined from the TG/DTG test.

TG/DTG test results showed some interesting trends among samples that highlight the differences between the SRW kind, binder dosage, curing atmosphere and curing time. Keeping the other variables constant, *P*2 combinations showed in general lower loss of mass related to the dehydration, dehydroxylation and decarbonation processes compared to *P*1. This could be related to the lower MgO content of this SRW, 41.11 %, compared to *P*1 with 76.13 %, that would maintain some reactivity and ability to hydrate, to create cementitious gels and to carbonate in presence of CO_2. As expected, for both SRW, hydration degree increased as the binder content did. No significant increase in hydration degree trends were observed from 7 to 28 days, revealing a rapid cementitious gels formation from the MgO of the binder that was completed before 7 days and a very low reactivity of the MgO (as periclase) from the SRW [23]. A direct relationship between the CO_2 content of the curing atmosphere and the hydration degree was observed. This suggests a positive effect of CO_2 curing for the cementitious gels formation and contradicts the results of Unluer and Al-Tabbaa [8] who observed that CO_2 curing consumed MgO for carbonation making it not available for the GGBS activation. Dehydroxylation did not show a direct relationship with the binder content, but a positive effect of the curing under 100 % CO_2 atmosphere on the dehydroxylation was observed. This showed that this curing method favored the formation of portlandite and brucite from the SRW while the CaO and MgO from the binder were probably spent for the cementitious gels formation at the earlier ages of the curing period. This effect was more intense in the *P*2 combinations and would be attributed to the highest content of CaO of this waste compared to *P*1. Direct relationships between the binder dosage and the decarbonation intensity, as well as between the curing time and the decarbonation intensity were observed for both SRW. *P*1 combinations did not show any relationships between the curing atmosphere and the carbonation degree as previously observed by Kim et al. [11], with the main decarbonation peak being attributed to the calcium carbonates decomposition [25]. As previously commented,

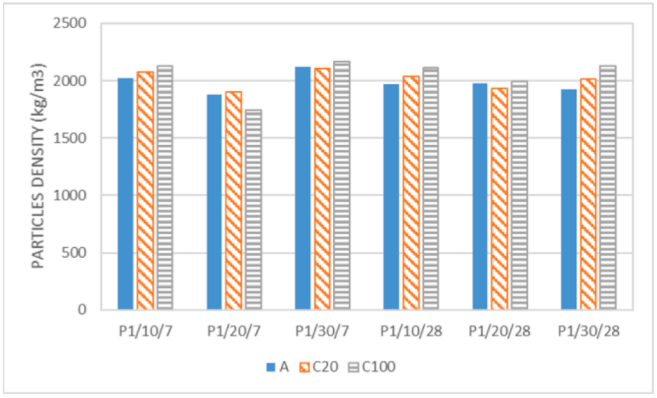

a)

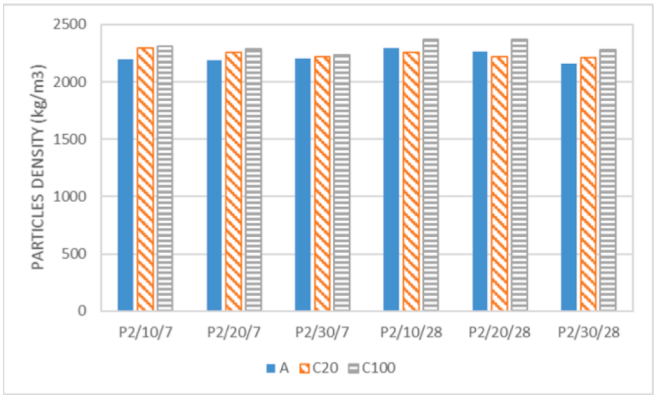

b)

Fig. 5. Particle densities of the aggregates manufactured in function of the atmosphere curing. a) *P*1 combinations and b) *P*2 combinations.

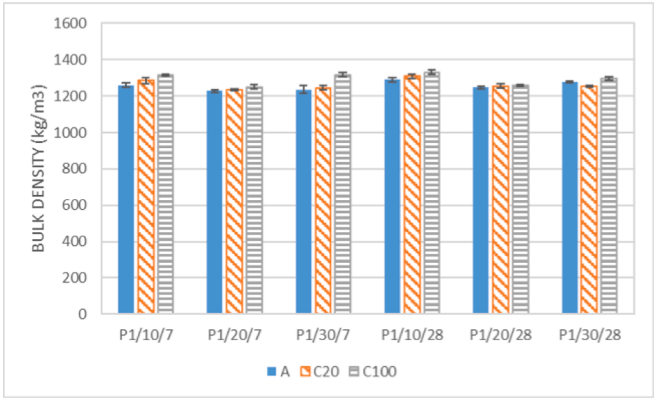

a)

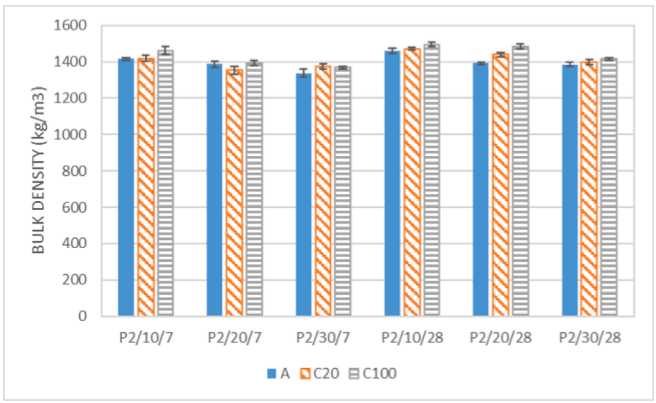

b)

Fig. 6. Bulk densities of the aggregates manufactured of atmosphere curing. a) *P*1 combinations and b) *P*2 combinations.

these combinations also showed a secondary peak in the carbonation zone of the DTG curves centered at the 550 °C, attributed to magnesium carbonates decomposition [23]. *P*2 combinations showed a direct relationship between the carbonation degree and the binder dosage as well as between the carbonation degree and the CO_2 content of the curing atmosphere. The peak at 550 °C was not clearly observed in the *P*2 combinations. These results suggest that an important amount of the decarbonation was due to the carbonates content of the PC-8 because of its manufacturing process [27]. The presence of the magnesium carbonate peak in the *P*1 samples, directly related to the binder content, independently of the curing atmosphere, suggests an origin of these carbonates from the binder. At the same curing ages and with the same binder dosages, *P*2 combinations showed higher contents of carbonates than *P*1 ones. Carbonation degree increased from 7 days to 28 days. A direct relationship between the curing atmosphere CO_2 content and carbonation mass loss was also observed. This revealed the higher ability of *P*2 combinations to uptake CO_2 and to produce calcium carbonates during the curing period.

3.3. Granulates physical properties

Figs. 5 and 6 show the particle densities and the bulk densities of the manufactured granulates at the ages of 7 and 28 days.

All the combinations reached relatively low values of particle densities and bulk densities compared to natural aggregates but in accordance with those obtained by Jiang and Ling [12] from steel-making slag granulation. *P*2 combinations showed higher particle densities and bulk densities compared to *P*1 ones. These differences were attributed to the coarser granulometry of the *P*2 and its higher content of iron oxide, compared to *P*1.

The *P*1 particle densities oscillated between 1,740 kg/m^3 and 2.,160 kg/m^3, corresponding to the combinations *P*1/20/7/100 and *P*1/30/7/100, respectively. No significant relationships were observed between particle density and binder dosage or curing age. Only a slight increase of the particle densities in the CO_2 curing atmospheres was observed. This fact could be attributed to the granulates manufacturing inhomogeneities, testing uncertainties, close particle densities achieved by the different samples, or overlapping effects of hydration and carbonation processes [11,12,16,25]. *P*2 particle densities oscillated in the range 2,160–2,370 kg/m^3, reached by the combinations *P*2/30/28/A and *P*2/20/28/100, respectively. *P*2 combinations achieved higher particle densities than *P*1 ones, probably based on the lower fine particles content or on the chemical composition of *P*2. Despite some inconsistent results that were attributed to the same reasons than in the case of the *P*1 combinations, *P*2 samples showed an indirect correlation between the particle density and the binder dosage. A direct relationship between the particle density and the curing CO_2 concentration was also observed.

*P*1 bulk densities oscillated between 1,230 kg/m^3 and 1,330 kg/m^3, reached by the combinations *P*1/20/7/A and *P*1/10/28/100 respectively. Direct relationships between the bulk density, the curing time and the CO_2 concentration of the curing atmosphere were observed. This effect was attributed to the carbonation process that would create a denser micro-structure, as observed by Mo and Panesar [25], Shi Ling y Guo [17] and Jiang y Ling [12]. Kim et al. [11] determined that an atmosphere containing a CO_2 concentration of 20 % was the optimum to get the densest and strongest carbonated MgO-GGBS structure. Tam et al. [28] observed an increase of the porosity and a decrease of the

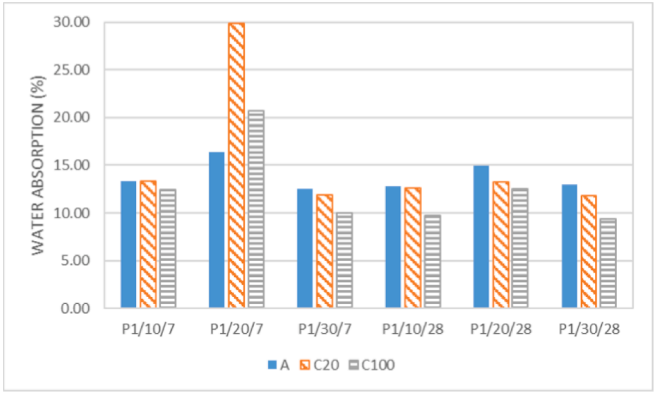

a)

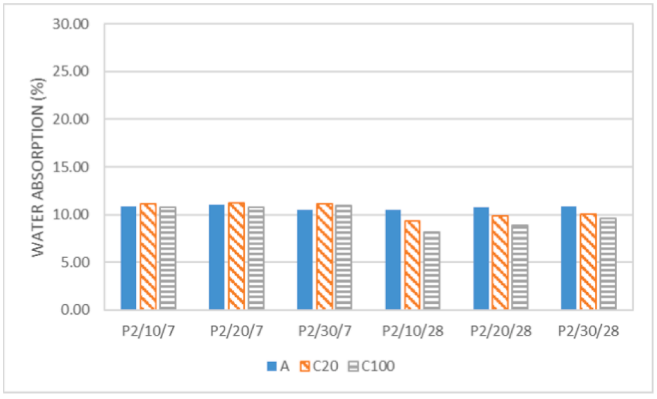

b)

Fig. 7. Water absorption of the granulates manufactured. a) *P*1 combinations and b) *P*2 combinations.

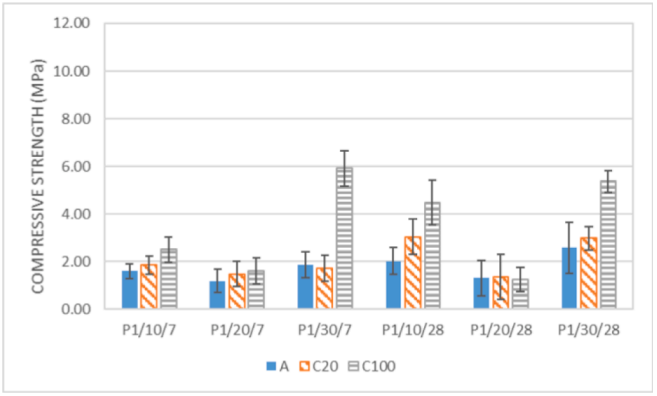

a)

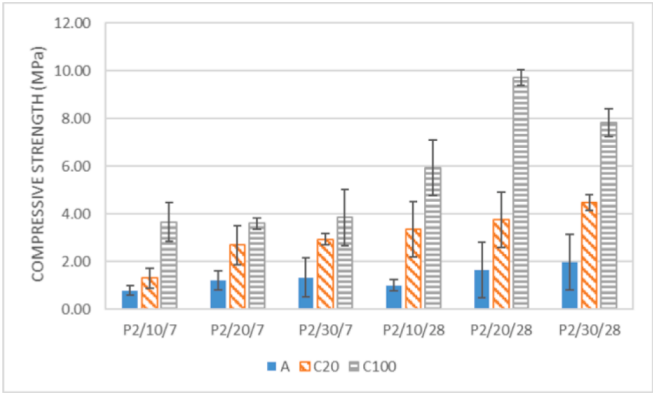

b)

Fig. 8. Compressive strength test results of the granulates manufactured. a) *P*1 combinations and b) *P*2 combinations.

strength of cement pastes due to carbonation. These contradictory results highlight the complexity of the effect of the binder hydration and carbonation. Both processes occur simultaneously in the CO_2 curing of granulates and the differences of materials used, manufacturing and curing conditions would justify the variability of the results achieved in different studies. An indirect relationship between the bulk density and the binder content was identified and it was attributed to the content of coarser particles of *P*2. Thus, *P*2 samples reached a minimum bulk density of 1,340 kg/m^3 corresponding to the combination *P*2/30/7/A, containing the highest binder proportion and cured in air. On the other hand, the maximum bulk density, 1,50 kg/m^3, was achieved by the combination *P*2/10/28/100, containing the lowest binder dosage, an atmosphere of 100 % CO_2 and the longest curing time.

These particle densities and bulk densities results show that combinations *P*1/10/28/A, *P*1/20/28/A, *P*1/20/28/C20, *P*1/20/28/C100 and *P*1/30/28/A fulfilled the requirement of particle density lower that 2000 kg/m^3 set in the standard EN 13055–1 to be considered lightweight aggregates for concrete, mortar and grout.Fig. 7 depicts the water absorption test results of the granulate combinations at the different curing ages.

*P*1 combinations achieved water absorptions in general between 9 % and 15 %. Only *P*1/20/7 combinations showed a different behavior with water absorptions between 16 % and 30 %. On the other hand, *P*2 combinations water absorptions oscillated between 8 % and 11 %. In general, a correlation between the decrease of the water absorption, the curing time and the CO_2 concentration was observed. These results agree with those obtained by Shi et al. [29] and were attributed to the reduction of porosity in the aggregates matrix due to the binder carbonation.

3.4. Granulates mechanical properties

Fig. 8 shows the compressive strength of the granulates manufactured.

Compressive strength oscillated between 0.79 MPa and 9.71 MPa, corresponding to the combinations *P*2/10/7/A and *P*2/20/28/100. These results agree with those obtained by other authors and are adequate for the substitution of natural aggregates in construction and environmental applications [11,12,15,17]. Carbonation showed a beneficial effect on the granulates compressive strength, more clearly for *P*2 combinations, mainly when curing was carried out in 100 % CO_2 atmosphere. Unexpectedly, *P*1 combinations did not show any direct relationship between the compressive strength and the binder content at any curing age or curing condition. Thus, for example, the combinations *P*1/10/28/20, *P*1/20/28/20 and *P*1/30/28/20, reached respectively mean compressive strengths of 3.04 MPa, 1.34 MPa and 2.97 MPa. The same was observed related to the curing time with no clear compressive strengths increase patterns from 7 to 28 days. Among the *P*1 combinations, the best compressive strengths were achieved by the combinations *P*1/30/7/100, with 5.92 MPa, *P*1/30/28/100, with 5.37 MPa and *P*1/10/28/100, with 4.48 MPa. Despite the uncertainties of the results, a decrease of the compressive strength seems to occur between the age of 7 days and 28 days in *P*1 samples cured in 100 % CO_2 atmosphere. It could be due to the formation of magnesium carbonates with a relatively weak structure or to the formation of expansive minerals that hinder the granulates strength [11]. *P*2 samples showed more predictable general behavior trends. Compressive strengths increased as the binder content did. For the same binder content, at the same curing age, compressive strength increased as the CO_2 concentration did. From 7 to 28 days, air

cured samples compressive strengths remained steady. On the other hand, for granulates cured in a CO_2 atmosphere the compressive strengths increased, mainly for the samples cured in 100 % CO_2 atmosphere. This demonstrates the beneficial effect of the carbonation of the granulates for their mechanical strength development.

4. Conclusions

This work analyzes the ability of two SRW with a binary MgO-GGBS hydraulic binder for the manufacturing of recycled granulates. Both SRW varieties demonstrated their potential to be used as target materials for producing granulates that accomplish the requirements for construction and environmental applications. SRW showed a residual reactivity that could benefit the manufacturing of recycled aggregates with improved properties. The empirical investigation carried out demonstrated the effectiveness of CO_2 curing conditions for the formation of cementitious gels and for the increase granulates carbonation degree that contributed to the reduction of the water absorption and to the increasing of the granulates compressive strength. Negative strength developments due to the formation of magnesium carbonate were not observed. Although the beneficial effects of the curing in CO_2 atmospheres were observed in the combinations of both SRW, their intensity was different based on their composition differences and reactiveness. This highlights the complexity of processes that overlap in the granulates strength development like cementation and carbonation. More investigations are required to get a better knowledge of the cementation and carbonation processes interaction in SRW granulates curing under different atmospheres.

Granulation process uncertainties also would require further analysis as potential source of granulate inhomogeneities. These manufacturing inhomogeneities probably were responsible of some unexpected results that contradicted the general trends observed in results obtained in this experimental investigation.

CRediT authorship contribution statement

A. Seco: Conceptualization, Methodology, Formal analysis, Writing – original draft, Writing – review & editing, Supervision. **J.M. del Castillo:** Methodology, Formal analysis, Investigation, Writing – original draft. **C. Perlot:** Investigation, Formal analysis, Writing – review & editing. **S. Marcelino:** Resources, Investigation, Visualization, Project administration. **S. Espuelas:** Investigation, Data curation, Formal analysis, Funding acquisition.

Declaration of Competing Interest

The authors declare that they have no known competing financial interests or personal relationships that could have appeared to influence the work reported in this paper.

Data availability

Data will be made available on request.

Acknowledgements

This work was funded by *Gobierno de Navarra* and *Fondo Europeo de Desarrollo Regional* (FEDER) by the *SUMIDERO VIAL CON SEPARACIÓN DE METALES PESADOS (SUMIDEEP)* (Reference: 0011-1365-2019-000108), research project.

References

[1] A.P. Silva, A.M. Segadães, R.A. Lopes, Castable systems designed with powders reclaimed from dismantled steel induction furnace refractory linings, Ceram. Int. 43 (2017) 5020–5031, https://doi.org/10.1016/j.ceramint.2017.01.012.

[2] L. Horckmans, P. Nielsen, P. Dierckx, A. Ducastel, Recycling of refractory bricks used in basic steelmaking: A review, Resour. Conserv. Recycl. 140 (2019) 297–304, https://doi.org/10.1016/j.resconrec.2018.09.025.

[3] European Commission, The EU Steel Industry, DG GROWTH - Internal Market, Industry, Entrepreneurship and SMEs. (2014). https://ec.europa.eu/growth/sectors/raw-materials/industries/metals/steel_en.

[4] A.G.M. Othman, W.M.N. Nour, Recycling of spent magnesite and ZAS bricks for the production of new basic refractories, Ceram. Int. 31 (2005) 1053–1059, https://doi.org/10.1016/j.ceramint.2004.11.004.

[5] A. van Zomeren, S.R. van der Laan, H.B.A. Kobesen, W.J.J. Huijgen, R.N. J. Comans, Changes in mineralogical and leaching properties of converter steel slag resulting from accelerated carbonation at low CO 2 pressure, Waste Manag. 31 (2011) 2236–2244, https://doi.org/10.1016/j.wasman.2011.05.022.

[6] M. Morone, G. Costa, A. Polettini, R. Pomi, R. Baciocchi, Valorization of steel slag by a combined carbonation and granulation treatment, Miner. Eng. 59 (2014) 82–90, https://doi.org/10.1016/j.mineng.2013.08.009.

[7] B. Pang, Z. Zhou, H. Xu, Utilization of carbonated and granulated steel slag aggregate in concrete, Constr. Build. Mater. 84 (2015) 454–467, https://doi.org/10.1016/j.conbuildmat.2015.03.008.

[8] C. Unluer, A. Al-Tabbaa, The role of brucite, ground granulated blastfurnace slag, and magnesium silicates in the carbonation and performance of MgO cements, Constr. Build. Mater. 94 (2015) 629–643, https://doi.org/10.1016/j.conbuildmat.2015.07.105.

[9] J. Yliniemi, H. Nugteren, M. Illikainen, M. Tiainen, R. Weststrate, J. Niinimäki, Lightweight aggregates produced by granulation of peat-wood fly ash with alkali activator, Int. J. Miner. Process. 149 (2016) 42–49, https://doi.org/10.1016/j.minpro.2016.02.006.

[10] Z. Ghouleh, R.I.L. Guthrie, Y. Shao, Production of carbonate aggregates using steel slag and carbon dioxide for carbon-negative concrete, J. CO2 Util. 18 (2017) 125–138, https://doi.org/10.1016/j.jcou.2017.01.009.

[11] T.Y. Kim, J.Y. Ahn, C. Kim, S.J. Choi, T.T. Ho, D.H. Moon, I. Hwang, Carbonation/granulation of mine tailings using a MgO/ground-granule blast-furnace-slag binder, J. Hazard. Mater. 378 (2019), 120760, https://doi.org/10.1016/j.jhazmat.2019.120760.

[12] Y. Jiang, T.C. Ling, Production of artificial aggregates from steel-making slag: Influences of accelerated carbonation during granulation and/or post-curing, J. CO2 Util. 36 (2020) 135–144, https://doi.org/10.1016/j.jcou.2019.11.009.

[13] S. Espuelas, J. Omer, S. Marcelino, A.M. Echeverría, A. Seco, Magnesium oxide as alternative binder for unfired clay bricks manufacturing, Appl. Clay Sci. 146 (2017), https://doi.org/10.1016/j.clay.2017.05.034.

[14] A. Seco, P. Urmeneta, E. Prieto, S. Marcelino, B. García, L. Miqueleiz, Estimated and real durability of unfired clay bricks: Determining factors and representativeness of the laboratory tests, Constr. Build. Mater. 131 (2017) 600–605, https://doi.org/10.1016/j.conbuildmat.2016.11.107.

[15] P.J. Gunning, C.D. Hills, P.J. Carey, Production of lightweight aggregate from industrial waste and carbon dioxide, Waste Manag. 29 (2009) 2722–2728, https://doi.org/10.1016/j.wasman.2009.05.021.

[16] H.Q.H. Phan, K.Y. Hwang, J.Y. Ahn, T.Y. Kim, C. Kim, I. Hwang, Investigation of the accelerated carbonation of a MgO-based binder used to treat contaminated sediment, Environ. Earth Sci. 76 (2017) 1–11, https://doi.org/10.1007/s12665-017-7115-6.

[17] M. Shi, T.C. Ling, B. Gan, M.Z. Guo, Turning concrete waste powder into carbonated artificial aggregates, Constr. Build. Mater. 199 (2019) 178–184, https://doi.org/10.1016/j.conbuildmat.2018.12.021.

[18] F.M. Mahdi, M. Mehrabi, A. Hassanpour, F.L. Muller, On the formation of core-shell granules in batch high shear granulators at two scales, Powder Technol. 356 (2019) 253–262, https://doi.org/10.1016/j.powtec.2019.08.019.

[19] H. Azrar, R. Zentar, N.E. Abriak, The Effect of Granulation Time of the Pan Granulation on the Characteristics of the Aggregates Containing Dunkirk Sediments, Procedia Eng. 143 (2016) 10–17, https://doi.org/10.1016/j.proeng.2016.06.002.

[20] S.M. Monteagudo, A. Moragues, J.C. Gálvez, M.J. Casati, E. Reyes, The degree of hydration assessment of blended cement pastes by differential thermal and thermogravimetric analysis. Morphological evolution of the solid phases, Thermochim. Acta 592 (2014) 37–51, https://doi.org/10.1016/j.tca.2014.08.008.

[21] F. Matalkah, P. Soroushian, Synthesis and characterization of alkali aluminosilicate hydraulic cement that meets standard requirements for general use, Constr. Build. Mater. 158 (2018) 42–49, https://doi.org/10.1016/j.conbuildmat.2017.10.002.

[22] D. Zhang, X. Cai, B. Jaworska, Effect of pre-carbonation hydration on long-term hydration of carbonation-cured cement-based materials, Constr. Build. Mater. 231 (2020), 117122, https://doi.org/10.1016/j.conbuildmat.2019.117122.

[23] K.Y. Hwang, J.Y. Seo, H.Q.H. Phan, J.Y. Ahn, I. Hwang, MgO-based binder for treating contaminated sediments: Characteristics of metal stabilization and mineral carbonation, Clean - Soil, Air, Water. 42 (2014) 355–363, https://doi.org/10.1002/clen.201200663.

[24] P. Westgate, R.J. Ball, K. Paine, Olivine as a reactive aggregate in lime mortars, Constr. Build. Mater. 195 (2019) 115–126, https://doi.org/10.1016/j.conbuildmat.2018.11.062.

[25] L. Mo, D.K. Panesar, Accelerated carbonation - A potential approach to sequester CO2 in cement paste containing slag and reactive MgO, Cem. Concr. Compos. 43 (2013) 69–77, https://doi.org/10.1016/j.cemconcomp.2013.07.001.

[26] P. Czapik, J. Zapała-Sławeta, Z. Owsiak, P. Stępień, Hydration of cement by-pass dust, Constr. Build. Mater. 231 (2020), https://doi.org/10.1016/j.conbuildmat.2019.117139.

[27] A. Seco, J.M. del Castillo, S. Espuelas, S. Marcelino, A.M. Echeverría, Assessment of the ability of MGO based binary binders for the substitution of Portland cement for

mortars manufacturing, Constr. Build. Mater. 341 (2022), 127777, https://doi.org/10.1016/j.conbuildmat.2022.127777.
[28] V.W.Y. Tam, K. Wang, C.M. Tam, Assessing relationships among properties of demolished concrete, recycled aggregate and recycled aggregate concrete using regression analysis, J. Hazard. Mater. 152 (2008) 703–714, https://doi.org/10.1016/j.jhazmat.2007.07.061.
[29] C. Shi, B. Qu, J.L. Provis, Recent progress in low-carbon binders, Cem. Concr. Res. 122 (2019) 227–250, https://doi.org/10.1016/j.cemconres.2019.05.009.